CHAPTER 4 SYNTHESIS AND CHARACTERIZATION OF EGGSHELL-DERIVED HYDROXYAPATITE

In this chapter, synthesis, and characterization of novel bioceramic material, i.e., hydroxyapatite (HAp) from waste eggshells, is experimentally produced using a modified synthesis route. Here, multi-stage calcination followed by the chemical precipitation method is used to synthesize high-yielding and pure HAp derived from waste eggshells. Phase transformation with calcination temperature (till 1150 ^{0}C) and Stirring timing (6 hr, 12 hr, 18 hr and 24 hr) are characterized. The optimization of chemical stirring timing and calcination temperature is done to finally claim the best process and product. Powder flow analysis using tap density, bulk density, angle of repose of powder, Hausner ratio and Carr's index reveals the "fair" flow property for HAP6Hr and HAP12Hr and "good" for HAP18Hr and HAP24Hr samples. Average particle size 39.33 ± 11.01 μm - 22.05 ± 06.72 μm), average crystalline size (505.09Å-555.54Å), average lattice strain (0.2697%-0.3050%), stoichiometric composition (Ca/P = 1.67), elemental & compound composition and material bonding are evaluated from histograms and curves obtained through instrumental characterizations. Morphology validation is done using SEM, EDS, FTIR and XRD characterizations. The results conclude the effective utilization of eggshell-derived HAp for biomedical applications.

4.1 Synthesis of Eggshell-derived HAp

Synthesis of biocompatible hydroxyapatite from waste eggshells that are disposed into the dustbin is done using multistage calcination and chemical precipitation method at four different stirring timings i.e. 6 hours, 12 hours, 18 hours and 24 hours and the

final HAp prepared are nomenclate as HAP06Hr, HAP12Hr, HAP18Hr and HAP24Hr, respectively. **Fig. 4.1 (a)** illustrates the step wise synthesis of HAp from waste eggshell. All the four compositions were prepared simultaneously as shown in **Fig. 4.1 (b).**

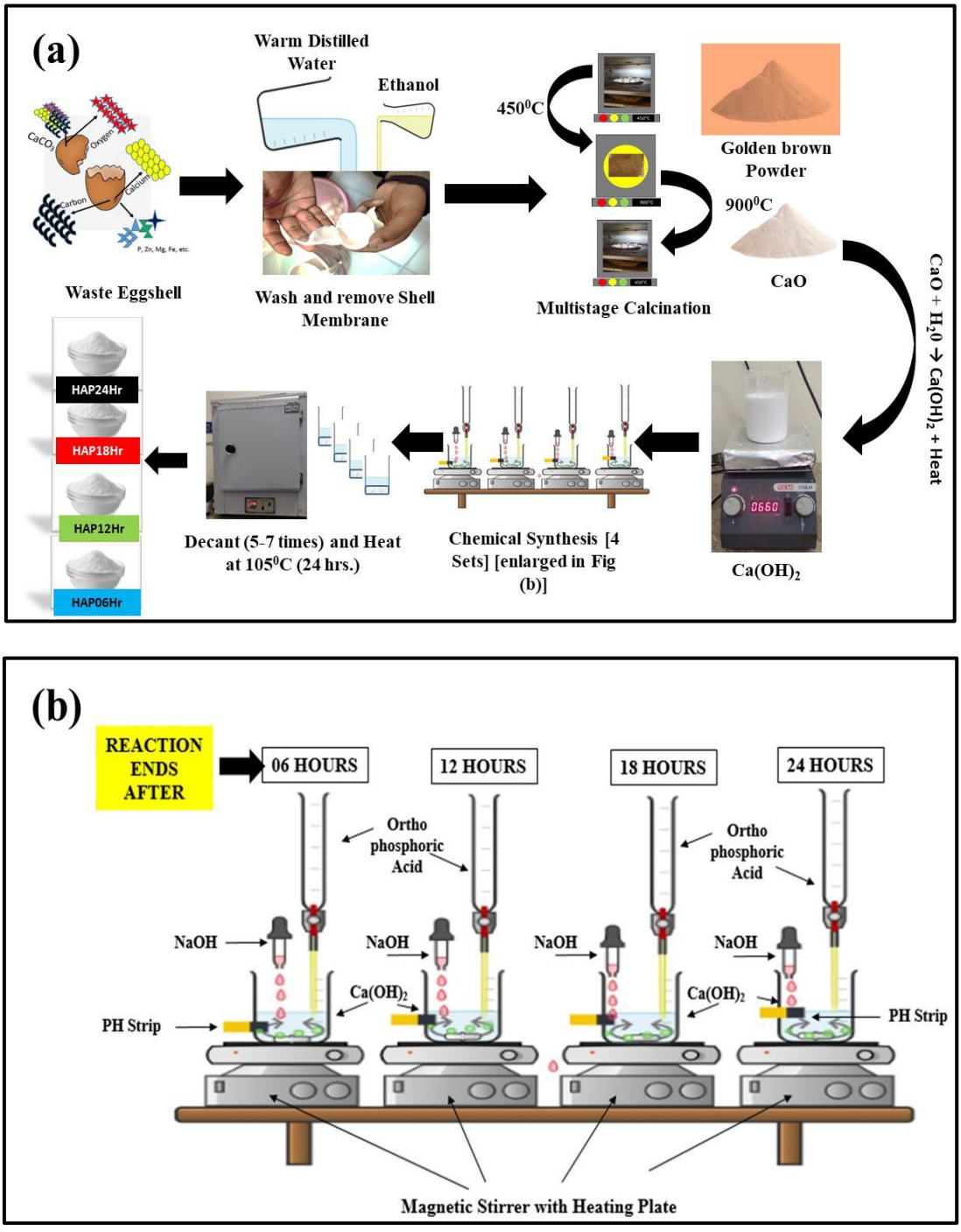

Fig. 4.1 (a) Systematic workflow for synthesis of optimized hydroxyapatite from waste eggshell, and (b) schematic experimental setup for simultaneous preparation of four samples of HAp.

The raw eggshells were washed using light warm distilled water and ethanol. Then the thin shell layer present between egg white and eggshell were removed. Cleaned eggshell were dried at the temperature of 405 ^{0}C with 50 ^{0}C/ min rate in the electric oven for 2 hours. The appearance of the eggshell turns golden brown and copper type color. After drying and when the temperature of the eggshell reached normal, the eggshells were crushed and sieved (100 – 250 microns), and converted to fine golden-brown powder. The powder at this stage contains almost 94% $CaCO_3$ and 6% other elements, compounds, and residues. Calcination of the powdered sample in the inert atmosphere with a temperature range of 750^{0}C – 1200^{0}C (keeping 900 ^{0}C as the standard temperature) was done in the muffle furnace for 4 hours. The golden-brown powder first turned black and when all the carbon and residues get calcinated it turned into white calcium rich oxide powder. Keep the calcium oxide powder (CaO) in a glass desiccator for 24hrs. Further, CaO was converted into $Ca(OH)_2$ by adding the methodical amount of water and stirring at 1100 rpm for 1 hour on the magnetic stirrer. Reaction is shown in equation (4.1). The reaction is exothermic, and the temperature of the prepared $Ca(OH)_2$ rises to 70 ^{0}C as measured. The conversion of calcium oxide to calcium hydroxide is essential as the solubility of $Ca(OH)_2$ is better in the acidic and water medium.

$$CaO + H_2O \rightarrow Ca(OH)_2 + Heat \quad \ldots (4.1)$$

After the conversion of CaO to $Ca(OH)_2$, the chemical precipitation process was performed for synthesis of 4 different HAp samples following the parameters listed in **Table 4.1.** using equation (b). **Figure 4.1 (b)** provides the elaborative pictorial view of the experimental setup utilized for the simultaneous synthesis of HAp during the chemical precipitation method.

$$10Ca(OH)_2 + 6H_3PO_4 \rightarrow Ca_{10}(PO_4)_6(OH)_2 + 18H_2O \quad \ldots (4.2)$$

After multistage heating and conversion of waste eggshell to calcium hydroxide, it was chemically treated to gain HAp. Magnetic stirrer, pH paper, temperature/ rpm regulator, NaOH (buffer solution to maintain pH in basic range (≥10), and orthophosphoric acid (poured at 5 mL/min) were used during the synthesis. The experimentation is done in similar environmental conditions and the reaction timing were varied with 6 h, 12 h, 18 h and 24 h magnetic stirring.

Table 4.1. Synthesis Parameters for Optimizing Reaction Rate.

Sample Name	Moles of Calcium based Compound	Moles of Phosphorous based Compound	pH	NaOH (M)	External Temperature Range (^{0}C)	Stirring Speed Range (RPM)	Reaction timing (Hours)
HAP06Hr	10	06	≥ 10	0.1	45 – 65	660 - 850	6
HAP12Hr	10	06	≥ 10	0.1	45 – 65	660 – 850	12
HAP18Hr	10	06	≥ 10	0.1	45 – 65	660 – 850	18
HAP24Hr	10	06	≥ 10	0.1	45 – 65	660 - 850	24

Multistage calcination is desired as the initial powdered sample of eggshell contains several elements and residues. The SEM-EDS of the powdered raw crushed eggshell is shown in **Fig. 4.2**. The calcium-rich (39.78 weight%) natural powdered sample contains elements including carbon, oxygen, sodium, magnesium, iron and zinc in varying weights and atomic percentages. Calcination is desired for the removal of carbon and other volatile impurities.

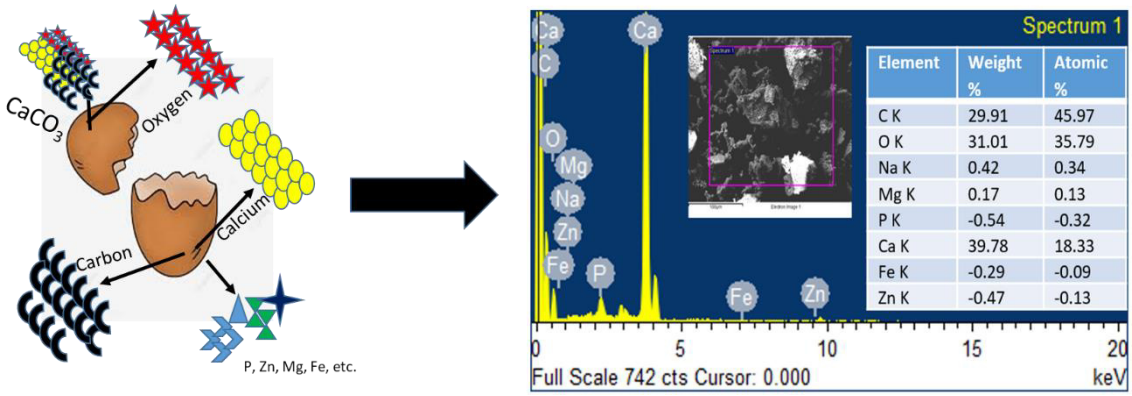

Fig. 4.2. Schematic of eggshell composition and Energy Dispersive X- Ray Spectroscopy of crushed eggshell.

The chemical precipitation process with precursors calcium hydroxide ($Ca(OH)_2$) derived from waste eggshells and orthophosphoric Acid (H_3PO_4) were performed simultaneously for synthesis of all four HAp samples. The Ca/P ratio is taken as 1.67 for attaining the HAp similar to inorganic component of human bone [20]. The rate of adding must be slower as adding higher amount of H_3PO_4 suddenly in the $Ca(OH)_2$ will solidify the product and creates a harmful exothermic reaction. It also impacts the stirring, pH and temperature of the reaction. The stirring timing after achieving the stoichiometric ratio (Ca/P = 1.67) is kept at 6, 12, 18 and 24 hours with final samples named as HAP06Hr, HAP12Hr, HAP18Hr and HAP24Hr, respectively. $Ca(OH)_2$ is weak base while H_3PO_4 being strong acid retains the PH between 3- 4 in the beginning of the reaction. Therefore, 0.1 M NaOH is desired in the beginning to raise the pH and once it crosses neutrality it remains constant. After that, multiple washing were performed and decanted the dispersion solution well with distilled water to remove the sodium and other impurities from the final solution. After complete washing, the solution was dried in electric oven at 105 ^{0}C at 5 ^{0}C for 8 hours. The finally synthesized HAp powdered samples obtained are shown in **Fig. 3.1 (Chapter 3).** The initial

appearance of the prepared samples shows milky white color, high level of crystallinity and effective flow property. The samples were then used for physical and morphological characterization.

4.2 Results and Discussions

4.2.1 XRD Analysis for multistage calcination

A multistage calcination process for the phase purity was performed on the waste eggshells. The refined XRD spectra with major compound peaks of the triturated and calcinated eggshell are shown in **Fig. 4.3 (a-g)**. In **Fig. 4.3 (a)** the major XRD peaks of washed, cleaned and calcinated crushed eggshells shows $CaCO_3$ along with other minor impurities. **Figure 4.3 (b)** shows XRD spectra of eggshell particles calcinated at 200 ^{0}C and it shows improved phases of $CaCO_3$ verified using JCPDS file No: 01-085- 0849. Its enlarged view with miller indices is shown in **Fig. 4.3 (h).** The XRD spectra of eggshell calcinated at 450 ^{0}C and 650 ^{0}C is illustrated in **Fig. 4.3 (c and d)**, and it shows the intermediate region between the decline of $CaCO_3$ and the rise of CaO peaks on heating. **Figure 4.3 (e)** shows calcination at 900 ^{0}C following the multistage calcination route, and the **Fig. 4.3 (f)** at 1150^{0}C, respectively. The enlarged view representing major peaks of CaO is shown in **Fig. 4.3 (i)**. The purest XRD spectra are visible and the sharp major CaO peaks are visible at two theta angles of 32.2^0, 37.34^0, 53.86^0, 64.14^0 and 67.36^0 as verified using JCPDS file no. 00- 037- 1497. Similar phases are observed at 900 ^{0}C and 1150 ^{0}C calcination, and therefore 900 ^{0}C is considered as optimum calcination temperature. Further, **Fig. 4.3 (g)** shows XRD spectra of eggshell calcinated directly from 0 to 900 ^{0}C with 5^{0}C/min heating rate. It shows peaks of $CaCO_3$ at 29.52^0 and 39.50^0 two theta angles that are high intensity peaks for $CaCO_3$. This phase impurity is due to improper calcination when done

directly at high temperatures. The XRD diffractogram confirms the phase purity with multistage calcination.

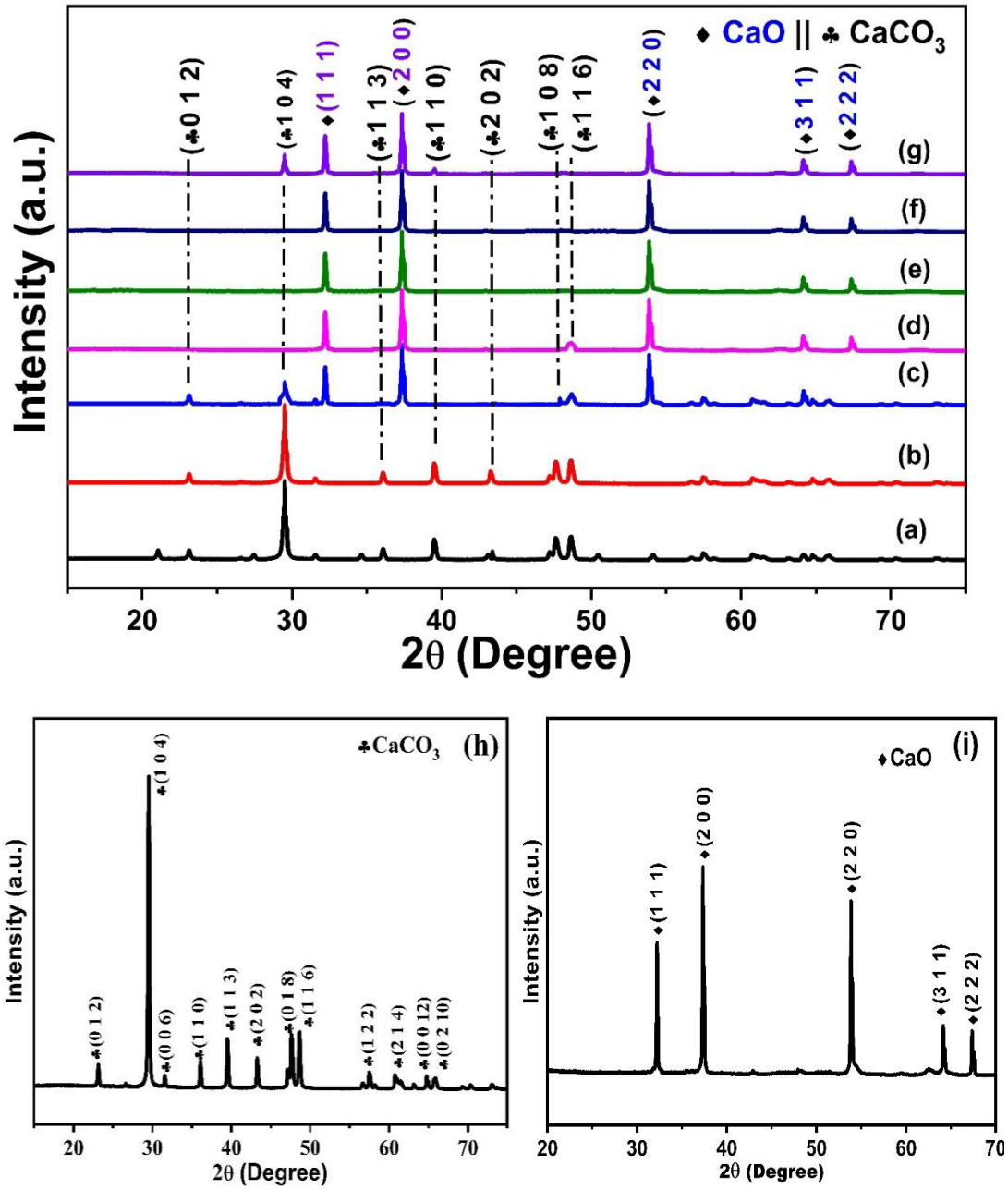

Fig. 4.3. XRD Spectra (a) Cleaned crushed eggshell, (b) eggshell calcinated at 200 ^{0}C, (c) 450 ^{0}C, (d) 650 ^{0}C, (e) 900 ^{0}C (during multistage calcination), (f) 1150 ^{0}C, (g) direct calcination to 900 ^{0}C, (h) pure $CaCO_3$, and (i) pure CaO.

4.2.2 Flow property of HAp Powder

To determine the flow property of the HAp samples, Hausner Ratio and Carr's Index was evaluated from the standard chart listed in **Table 3.5.** It is interesting to note that

the Hausner Ratio and Carr's Index of HAP18Hr is 1.13 and 11.25, respectively, which falls in the range of "**good flow"** property i.e. 1.12- 1.18 and 11- 15. The obtained results of flow property are tabulated in **Table 4.2.**

Results interpret the increase in tap density with increase in the stirring timing. The maximum value of tap density of HAp i.e. 1.89 was observed for HAP24Hr which is 2.717% higher than HAP18Hr (**Fig. 4.4 (a)**). A longer stirring period can help the HAp structure densify by minimizing the amount of pores and spaces in the substance. The variation in Hausner's ratio and Carr's index is observed in **Fig. 4.4 (b)**. The decrease in porosity improves the tap density by reducing the amount of vacant space within the particle arrangement. Good flowability of powdered samples is of the utmost importance for establishing accuracy, productivity, and uniformity in biomedical manufacturing procedures, thereby aiding in the creation of secure, efficient, and dependable medical goods and therapies [150,151]. The good flowability of the biocompatible biomaterials provides intense effectiveness in the manufacturing of biopaste, biolubricant and biocoating.

The experimental density of the eggshell-derived HAp was measured using Archimedes principle. The obtained results reports the experimental density for HAP06Hr, HAP12Hr, HAP18Hr and HAP24Hr was 2.66 ± .09, 2.74 ± 0.13, 2.84 ± 0.12 and 2.84 ± 0.16 g/cm^3 , respectively. Also, the theoretical density of pure and biocompatible HAp powder is 3.16 g/cm^3. The increase in densification for the similar chemical composition of HAp material but change in stirring timing concludes the increasing purity of synthesized HAp. The maximum relative density of 90.15 ± 0.63 % was observed in HAP24Hr. Also, the decrease in porosity was observed from 15.6 % (HAP06Hr) to 9.8 % (at and after 18 h stirring timing) (**Fig. 4.4 (d)**). According to Morgan et al. cortical bone i.e. the dense bone of human body has 5-15% porosity

[152], therefore attaining 9.8% porosity for HAP18Hr can be considered acceptable for orthopedic applications. Also, the relative density shows ≥ 90% at higher stirring timing. The densification also promoted the strength and surface hardness of the HAp material.

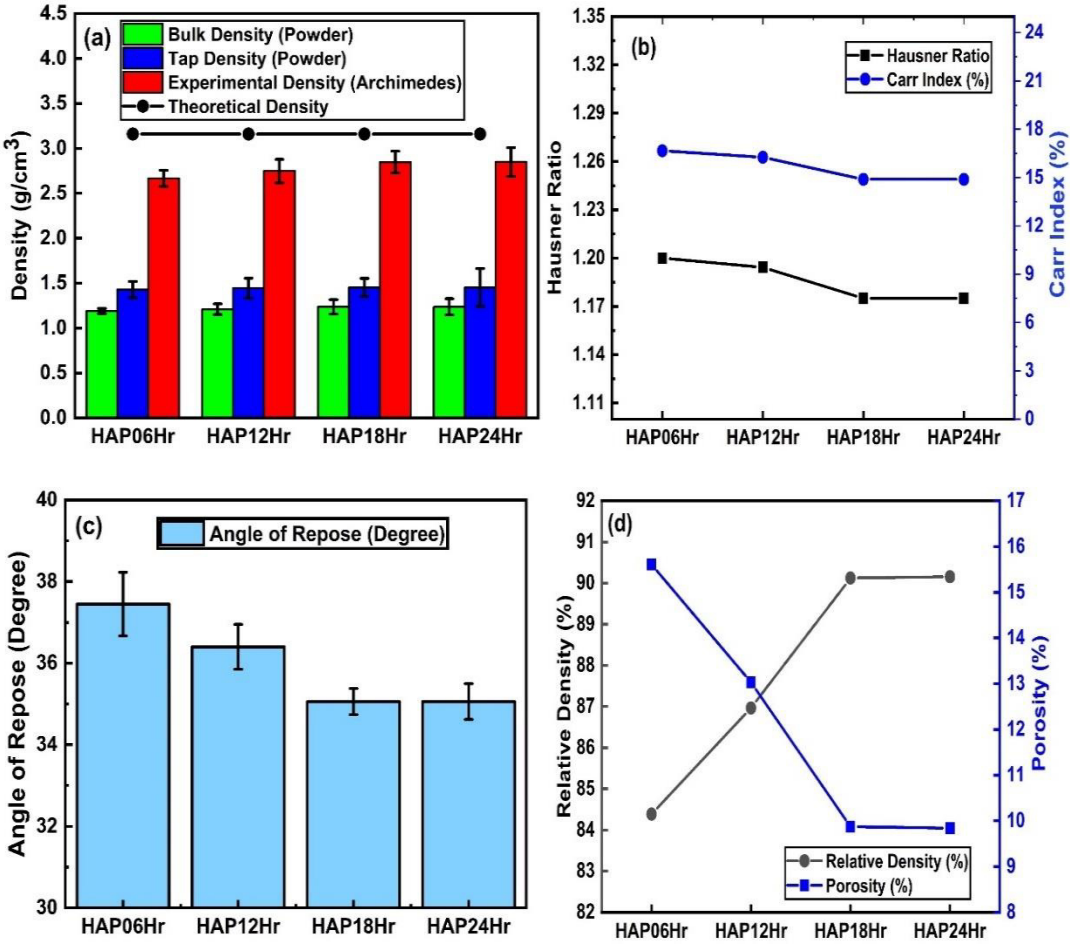

Fig. 4.4 (a) Experimental, theoretical, powder bulk and powder tap density, (b) Hausner's Ratio and Carr Index, (c) Angle of repose, and (d) Relative density and porosity percentage of eggshell-derived HAp at different stirring timings.

Table 4.2. Flow property, mass density and porosity % of HAp at different stirring timings.

Sample	Bulk Density (gm/cm^3)	Tap Density (gm/cm^3)	Angle of Repose	Carr's Index	Hausner Ratio	Flow	Theoretical Density	Experimental Density (Archimedes Principle)	Relative Density	Porosity %
HAP06HR	1.19 ± 0.03	1.43 ± 0.09	37.45 ± 0.78	16.666	1.20	FAIR	3.16	2.66 ± .09	84.39 ± 0.88	15.61 ± 0.44
HAP12HR	1.21 ± 0.06	1.44 ± 0.11	36.4 ± 0.55	16.263	1.194	FAIR	3.16	2.74 ± 0.13	86.97 ± 1.03	13.03 ± 1.22

HAP18HR	1.24 ± 0.08	1.45 ± 0.10	35.06 ± 0.32	14.893	1.175	GOOD	3.16	2.84 ± 0.12	90.12 ± 1.12	9.87 ± 0.56
HAP24HR	1.24 ± 0.09	1.45 ± 0.21	35.06 ± 0.44	14.893	1.175	GOOD	3.16	2.84 ± 0.16	90.15 ± 0.63	9.84 ± 1.11

The **Table 4.2** outlines the results obtained for the angle of repose of the HAP06Hr, HAP12Hr, HAP18Hr and HAP24Hr tested experimentally. The average of the two iterations is matched with the standard range. The experimental results are shown in **Fig. 4.4 (c)**. HAP06Hr and HAP12Hr powdered samples show fair flow property whereas HAP18Hr and HAP24Hr show good flow property. The improvement in the crystallinity and refinement in the grain size with increased stirring timing enhances the flow property of HAp. HAP18Hr shows 36.06^0 angle of repose during both the iterations. Flow properties are further evaluated using Hausner Ratio and Carr's Index.

4.2.3 Morphology Characterization

4.2.3.1 Scanning electron micrographs

The scanning electron micrographs of the eggshell powder, eggshell calcinated at 900 ^{0}C, HAP06Hr, HAP12Hr, HAP18Hr and HAP24Hr are shown in **Fig. 4.5 (a-f).** As observed, the calcinated eggshell powder forms acicular and irregular shapes (**Fig. 4.5 (b)**) and when it is synthesized to HAp after 6 hours magnetic stirring the obtained shape is flakey and angular (**Fig. 4.5 (c)**). However the multilayer smooth shape was observed for HAP12Hr powder (**Fig. 4.5 (d)**) and the flower-like morphology (**Fig. 4.5 (e)**) was observed for HAP18Hr powdered sample. Also, the multilayered flower-like morphology was observed for HAP24Hr (**Fig. 4.5 (f)**) which resembles with the morphology analysis of HAp done by Zhang et al. [153]. The SEM micrographs shown in **Fig. 4.6** was taken at 100 μm to identify the particle size of the powdered samples. The 20 different linear measurements per image were taken to illustrate the average particle size of the HAp powder. The histogram indicated in **Fig. 4.7 (a-d)** concludes

the normalization of particle size for synthesized eggshell-derived HAp at varying stirring timings.

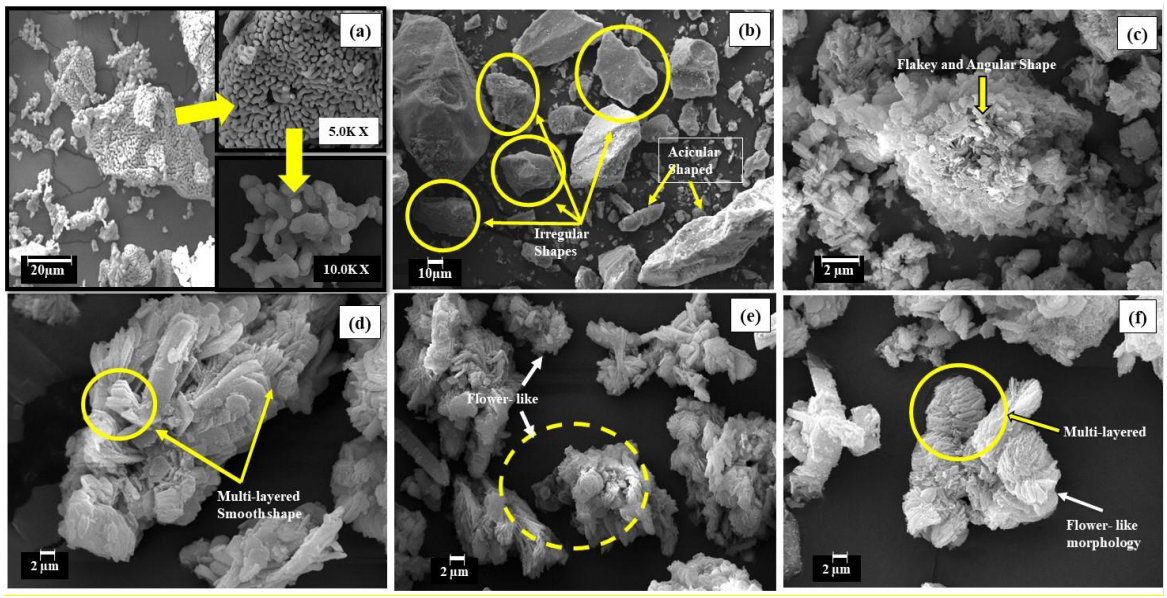

Fig. 4.5. Scanning Electron Morphology of (a) Crushed Eggshell, (b) Eggshell powder calcinated at 900^0C, (c) HAP06Hr, (d) HAP12Hr, (e) HAP18Hr and (f) HAP24Hr.

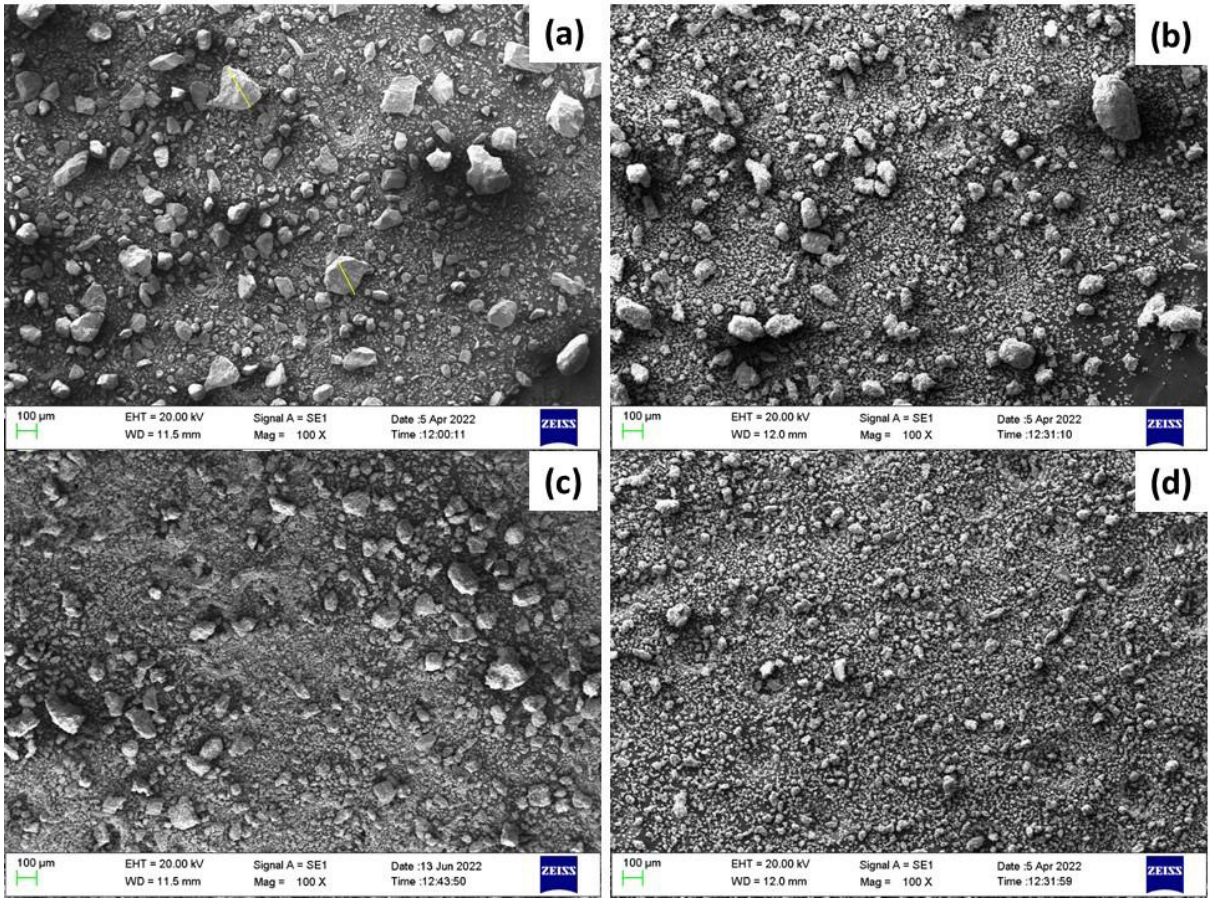

Fig. 4.6. SEM images to diagnose the particle size of (a) HAP06Hr, (b) HAP12Hr, (c) HAP18Hr and (d) HAP24Hr.

The APS for HAP06Hr, HAP12Hr, HAP18Hr and HAP24Hr are 39.33 ± 11.01 µm, 33.87 ± 14.79 µm, 22.27 ± 06.92 µm and 22.05 ± 06.72 µm, respectively **(Table 4.3)**. The decrease in APS with increase in stirring timings was monitored and almost 43.93 % decrease in APS was observed between HAP06Hr and HAP24Hr. Also, the uniform APS (≥ 1%) was observed when the synthesis was done above 18 h in the preparation of HAp. The main reason for the decrease in particle size with increase in stirring timing could be the improved homogenization, superior attrition and particle breakdown. The obtained particle size is well accepted in biomedical and implant coating applications.

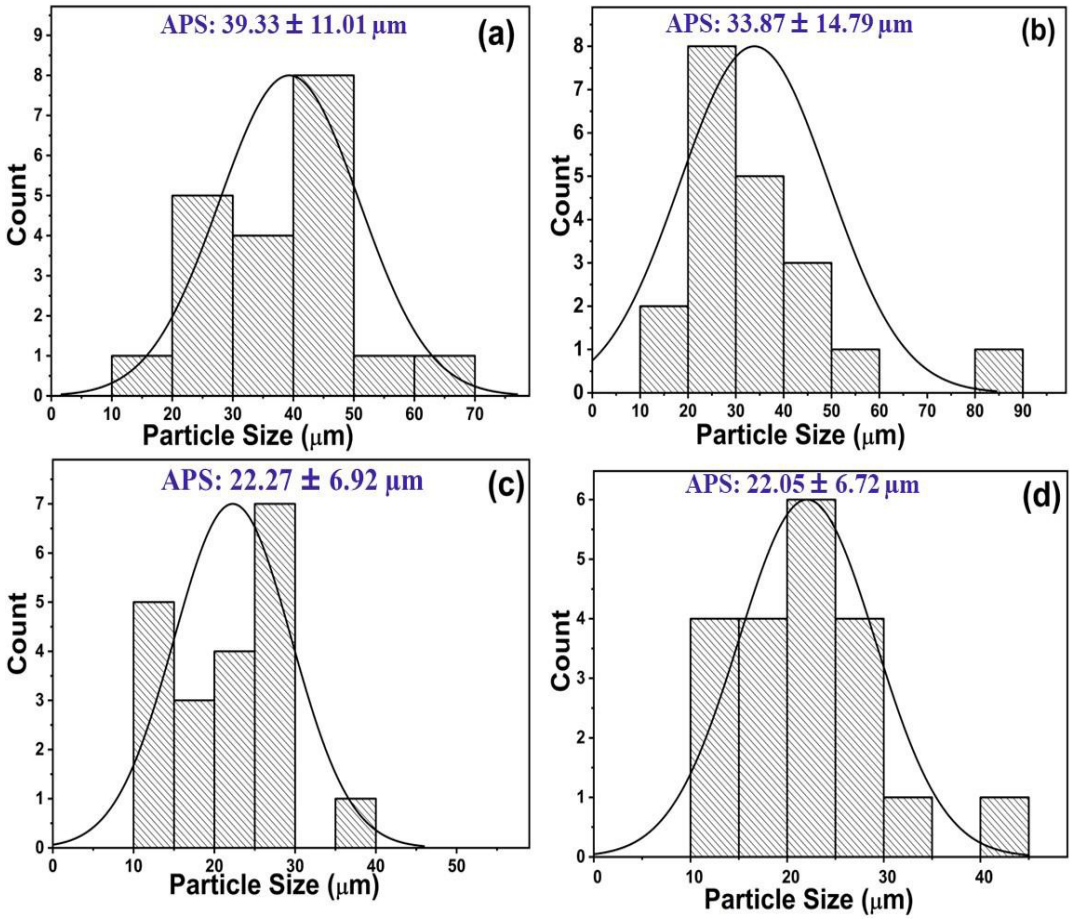

Fig. 4.7. Particle Size Analysis using Histogram graph of hydroxyapatite (a) HAP06Hr, (b) HAP12Hr, (c) HAP18Hr and (d) HAP24Hr.

Using SEM- EDS characterization, the elements diagnosed are Oxygen, Phosphorous and Calcium, and the weight % and atomic % for all the elements are mentioned in as

shown in **Fig. 4.8 (a-d).** The formation of strong appetite with high yielding rate (almost 50%) is synthesized using the chemical precipitation process with 24 h magnetic stirring and constant pH 10. The strong presence of Ca and P in the HAp formation is effectively visible in the EDS spectra. The elemental confirmation is verified using FTIR spectroscopy. The results also confirm the formation of HAp compounds with Ca, P and O which is verified using the obtained XRD peaks. Samples exhibited Ca/P ratio of 1.5954, 1.6137, 1.668 and 1.666 for HAP06Hr, HAP12Hr, HAP18Hr and HAP24Hr, respectively. It is interesting to note that stoichiometric ratio 1.67 is desired for the application of HAp in biomedical applications [154]. Therefore, HAP18Hr and HAP24Hr can be taken suitable for orthopedic biomedical applications.

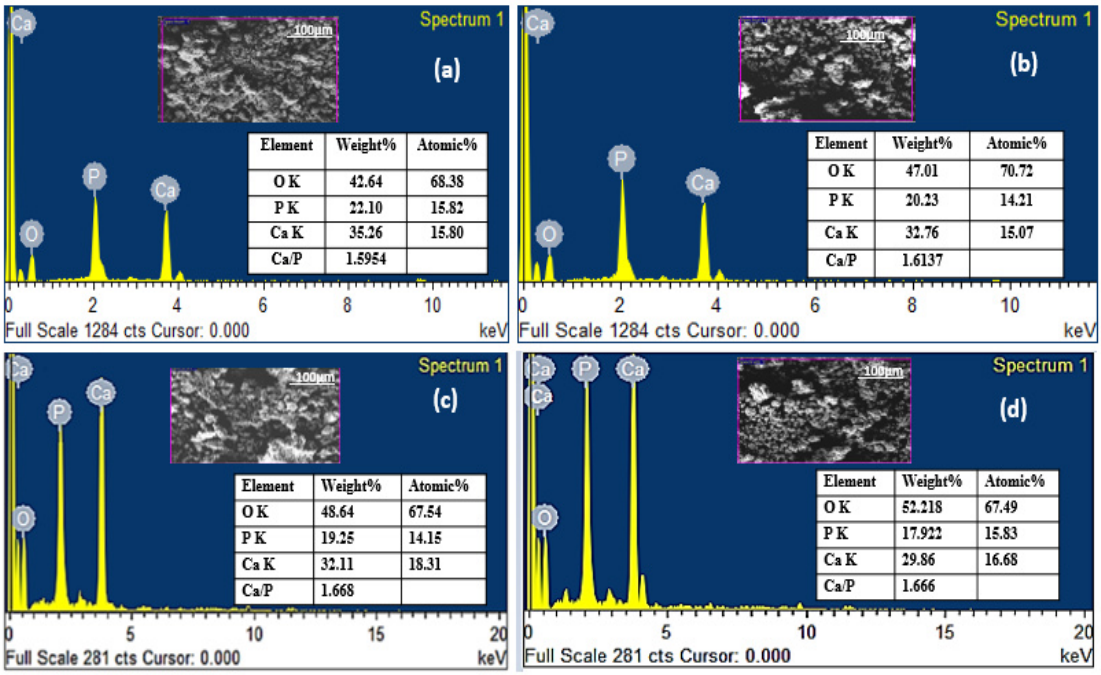

Fig. 4.8. SEM- Energy Dispersive Spectroscopy of the hydroxyapatite (a) HAP06Hr, (b) HAP12Hr, (c) HAP18Hr and (d) HAP24Hr.

4.2.3.2 X- Ray Diffraction Technique

Figure 4.9 illustrates the X- Ray diffractogram of all the HAp variations i.e. HAP06Hr, HAP12Hr, HAP18Hr and HAP24Hr. The obtained crystallographic curve contains compounds that matches with standard JCPDS file of Hexagonal Calcium

Hydroxyapatite ($Ca_{10}(PO4)_6(OH)_2$, (HAp (2)), JCPDS No: 01-074-0565), Penta Calcium tri phosphate Hydroxyapatite ($Ca_5(PO4)_3(OH)$, (HAP), JCPDS No: 01-086-0740) and Calcium Hydroxyl Phosphate (CHP) (Monetite structure, JCPDS No. 00-00-90080). Similar diffraction peaks for all samples reflects the stable crystalline structure of HAp [155]. Nejati et al. [156] reported similar XRD peaks for nano HAp rods when used with PLA for bone tissue engineering. The line pattern available in JCPDS files are used to locate the CHP and HAp in the XRD diffractogram. As observed, the initial 2θ phase contains CHP only and the clear peak is visible at 13.125^0 with 6.64Å d-spacing and (0 1 0) miller indices (referred from JCPDS No. 00-00-90080). The results are verified. The crystallite size at 13.125^0 is 615 Å, 742 Å, 537 Å and 537 Å for HAP06Hr, HAP12Hr, HAP18Hr and HAP24Hr, respectively as seen in **Fig. 4.9**. The sharp diffractogram peaks conclude the clear conversion of amorphous eggshell waste to crystalline HAP.

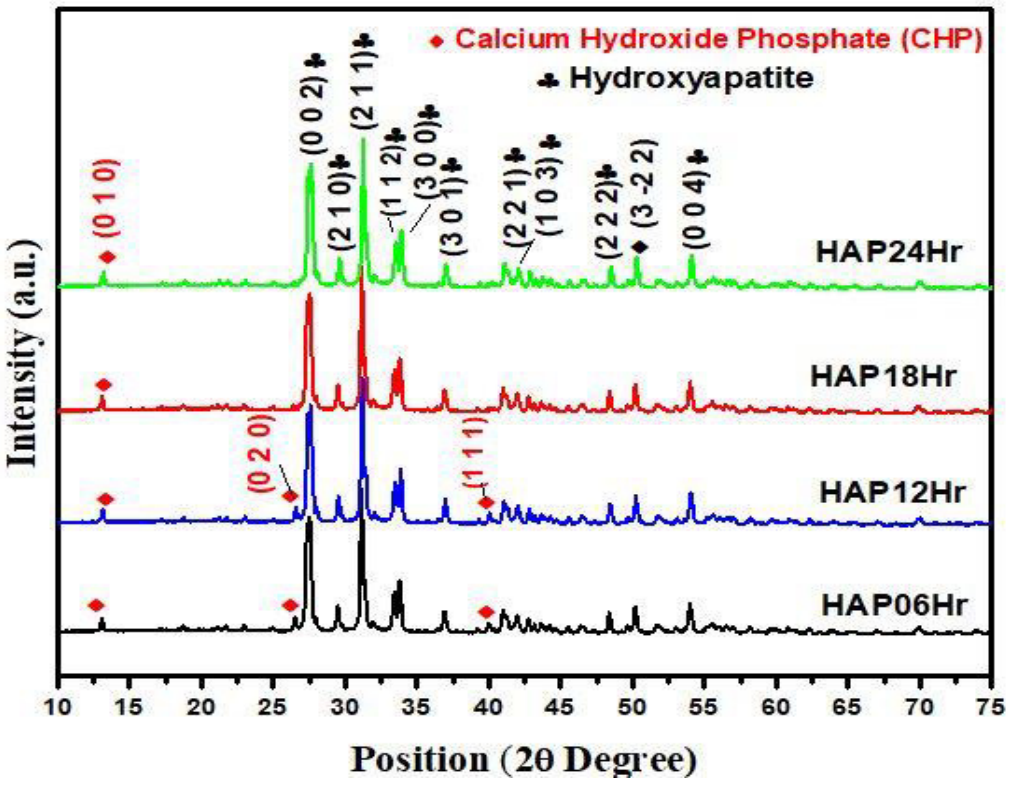

Fig. 4.9. X-Ray Diffractogram of the synthesized hydroxyapatite (a) HAP06Hr, (b) HAP12Hr, (c) HAP18Hr and (d) HAP24Hr.

Above 50^0 peak positions (2θ values) all the low and high intensity XRD peaks show pure HAp compound formation. The conversion of CHP to HAp is improved with the stirring timing and shows pure HAp crystallite structure for HAP18Hr and HAP24Hr.

4.2.3.3 Average Crystallite Size and Average Crystallite Strain

The crystallite size (in **Å**) (**Fig. 4.10)** and the lateral strain percentage (**Fig. 4.11**) for all the HAp samples are obtained using Scherer's equation (equation (k)) tool in XPert Highscore software for each peak individually are depicted from the XRD curve. Input parameters like two-theta (2θ) peak position**,** corresponding FWHM value and standard machine error (0.008) are attained using XRD Diffractogram. The average crystallite size and average lattice strain of all the four samples are tabulated in **Table 4.3.** The results show that HAP18Hr has a minimum average crystallite size of 505.09Å and 0.3050% average lateral strain whereas HAP06Hr has maximum average crystallite size (555.54Å) with 0.2964% lateral strain. The tolerance limit of crystallite size (±10 Å) indicates approximately similar crystallite size of HAP18Hr and HAP24Hr.

Table 4.3. Average Crystalline Size [Å], Lattice Strain (%) and Particle Size (nm) of the Hydroxyapatite Samples.

Sample	Average Crystallite Size [Å]	Average Lattice Strain (%)	Average Particle Size (µm)
HAP06Hr	555.54 ± 10	0.2964 ± 0.02	39.33 ± 11.01
HAP12Hr	537.09- ± 10	0.2697 ± 0.02	33.87 ± 14.79
HAP18Hr	505.09 ± 10	0.3050 ± 0.02	22.27 ± 06.92
HAP24Hr	513.54 ± 10	0.3012 ± 0.02	22.05 ± 06.72

The minor decrease in crystallite size is observed with increased stirring timings and reaction rate. The crystallite size in microns is approximately 0.5µm for all the HAp samples. The variation in lateral strain for HAP06Hr, HAP12Hr, HAP18Hr and HAP24Hr are shown in **Fig. 4.11 (a- d)** and the average lateral strain are tabulated in **Table 4.3**. The average particle size for HAP18Hr and HAP24Hr has less than 1 µm difference which outlines the uniform particle size at higher stirring timings. Also, the size of the particle decreases as the synthesis time is increased from 6 hours (Average particle size 39.33 ± 11.01 µm) to 24 hours (Average particle size 22.05 ± 06.72 µm).

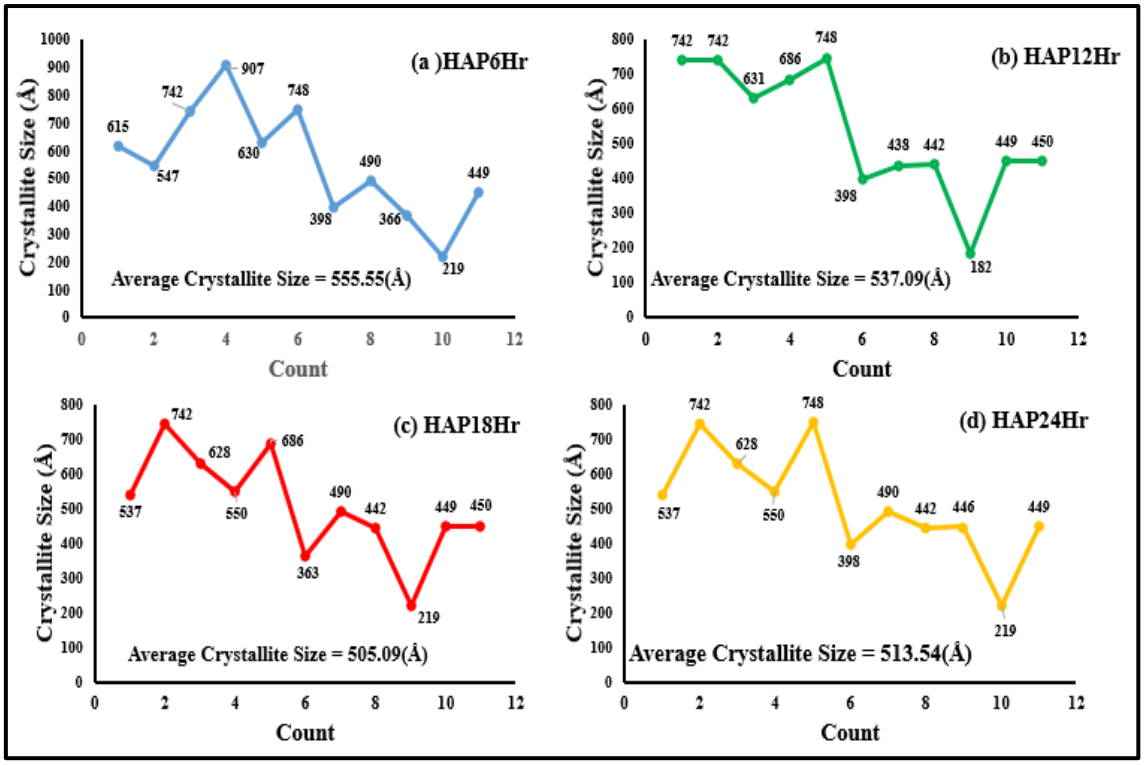

Fig. 4.10. Crystallite Size (in Å) of the synthesized hydroxyapatite **(a)** HAP06Hr, **(b)** HAP12Hr, **(c)** HAP18Hr and **(d)** HAP24Hr samples.

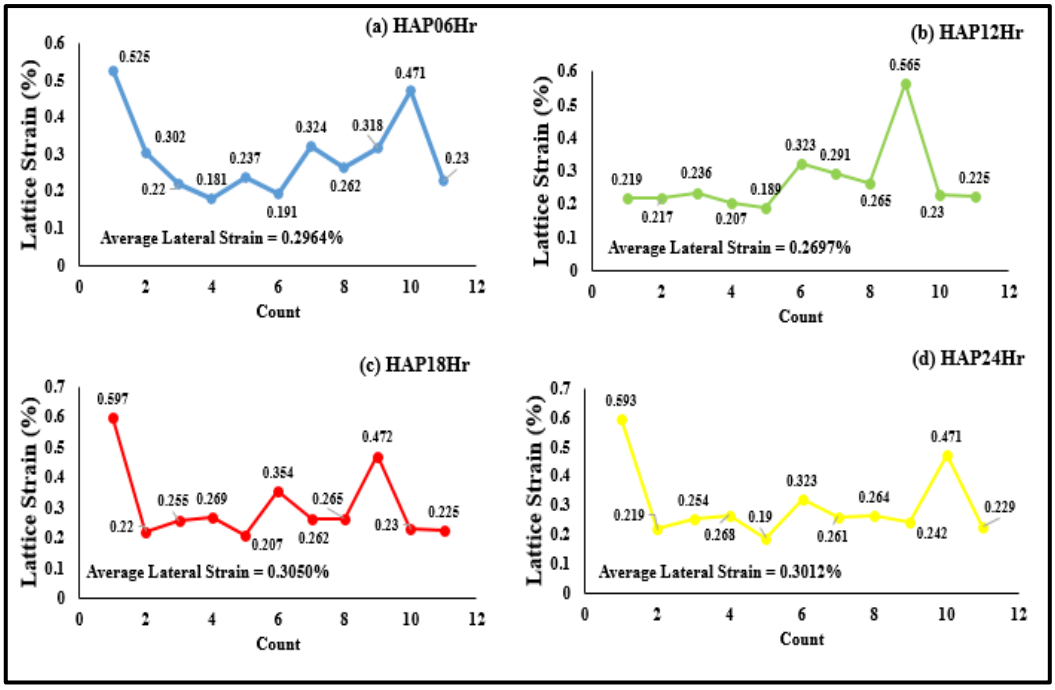

Fig. 4.11. Lattice Strain (%) of the synthesized hydroxyapatite **(a)** HAP06Hr, **(b)** HAP12Hr, **(c)** HAP18Hr and **(d)** HAP24Hr samples.

4.2.3.4 Fourier Transform Infrared Spectroscopy (FTIR)

Transmittance curves for four samples HAP06Hr, HAP12Hr, HAP18Hr and HAP24Hr with varying wave number obtained through FTIR spectra are shown in **Fig. 4.12**. The fingerprint region (500- 1500cm^{-1}) is undoubtedly visible. The transmittance curve between 3550cm^{-1} and 3230cm^{-1} reflects the presence of effective hydroxyl stretching (O-H) functional group in the apatite formation as the entire synthesis is carried out at basic PH = 10. The similar formation is reported by Lochaiwatana et al. [157] during synthesis of fluoridated HAP. The OH functional group occurs at wave number 3332.87cm^{-1} (HAP6Hr), 3333.83 cm^{-1} (HAP12Hr), 3329.01 cm^{-1} (HAP18Hr) and 3334.82 cm^{-1} (HAP24Hr). Fern and Salimi [158] reported OH functional group of synthesized HAp at 3400cm^{-1} and PO_4^{3-} near 1020 cm^{-1} that correlates closely with the current graph. As observed, the HAP18Hr imitates minimum value of wavenumber for the entire range of transmittance which interprets the optimum reaction timing for the formation of HAp. The steadfast HAp compound formation is seen between 850-

1150cm^{-1} with the transmittance peaks ranging from 30.2% (for HAP18Hr at 1150.33cm^{-1}) to 57.8% (for HAP06Hr at 850.45cm^{-1}). HAP18Hr shows maximum absorbance according to FTIR characterization.

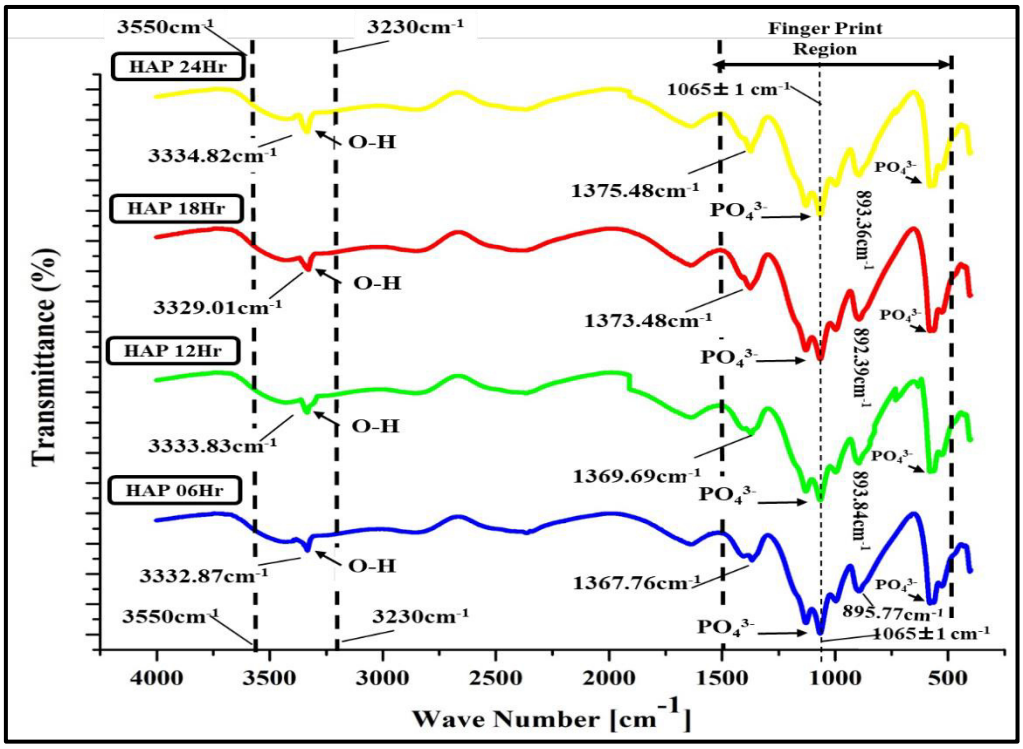

Fig. 4.12. Fourier Transform Infrared Spectroscopy (FTIR) of the eggshell-derived hydroxyapatite samples.

Vibration mode with asymmetric bending at 1165 ± 1cm^{-1} and asymmetrical stretching at 568 ± 1cm^{-1} mode displays PO_4^{-3} functional group for all the variations of samples and confirms the HAp formation in all the samples. The FTIR spectrograph resembles with the [159] and confirms the presence of functional groups and bonding desired in HAp formation. Hence, the synthesis of stable, crystalline, and pure HAp is verified using multiple morphological characterizations.

4.2.4 Wettability Analysis

4.2.4.1 Contact Angle Measurement

The hydrophilicity/ hydrophobicity of the synthesized HAp samples was experimentally determined using contact angle measurement machine (Model: DSA

25S, Kruss, Germany) using ASTM D5946 standard. The average of 5 readings per sample were obtained and graphed as shown in **Fig. 4.13**. The CA of HAP06Hr, HAP12Hr, HAP18Hr and HAP24Hr samples is $49.75^0 \pm 4.65^0$, $58.55^0 \pm 9.45^0$, $66.2^0 \pm 2.8^0$ and $66.75^0 \pm 2.45^0$, respectively (**Table 4.4**). It was observed that, the CA of the HAp samples increases with the increase in stirring timings. The increase of 17^0 between HAP06Hr and HAP24Hr depicts the comparative enhancement in hydrophobicity and the result further corelates with the decrease in water absorption percentage, porosity % and surface hardness [160]. Therefore, it can also be inferred that the contact angle not only relates to wettability but also governs the surface strength and biocompatibility of the fabricated HAp samples. According to Maidaniuc et al. [161] the decrease in particle size of the compacted samples governs the manipulation in wettability and as the particle size decreases with stirring timing of the synthesized HAp, the slight decrease in hydrophilicity was observed. Also, Eraković et al. [162] performed wettability analysis of silver-doped HAp using SBF sessile droplet and observed the hydrophilic nature (CA = $35.03° \pm 8.07^0$) and concludes that the wettability affects the blood coagulation, platelet adhesion/activation, protein adsorption and cell adhesion therefore the hydrophilic nature of HAp also marks an important role in an implant design.

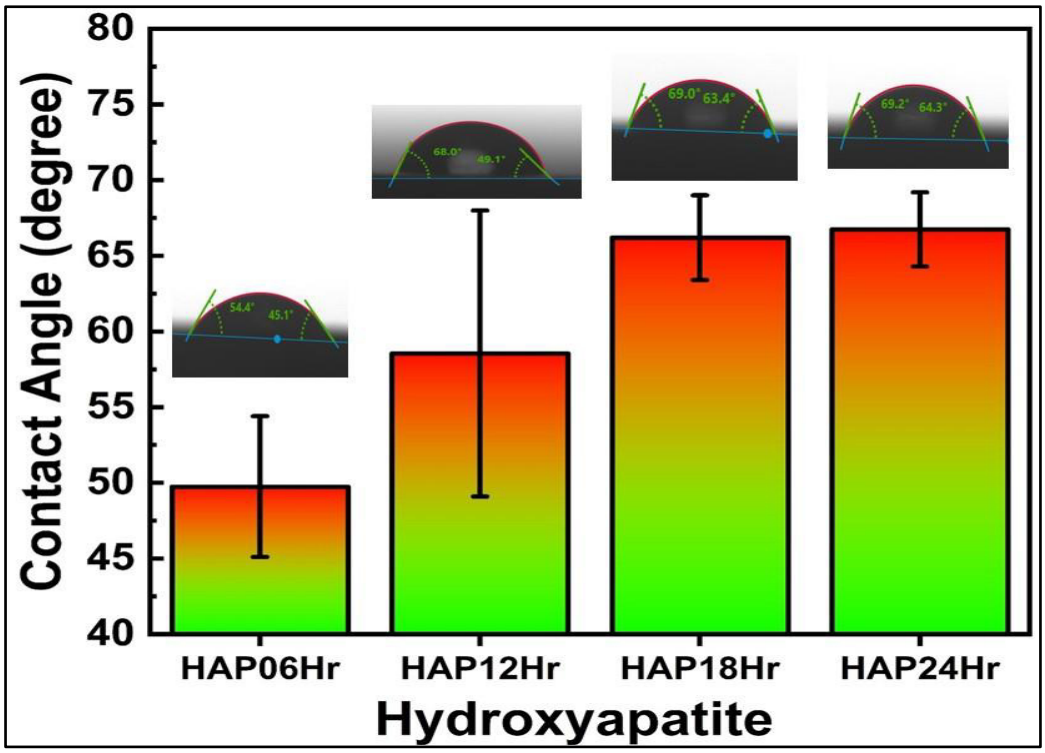

Fig. 4.13. Contact angle of eggshell-derived HAp at different stirring timings.

Table 4.4. Average Contact angle of HAp samples.

SAMPLE	Average Contact Angle	Standard Deviation
HAP06Hr	49.75	4.65
HAP12Hr	58.55	9.45
HAP18Hr	66.2	2.8
HAP24Hr	66.75	2.45

4.2.4.2 Water Absorption test

The wettability analysis of the HAp samples was examined through water absorption test using ASTM D 570-98 standard, at environmental temp of ≈ 40 ^{0}C and ≈ 51% RH. The samples were soaked in distilled water for 6 days and weighed after every 8 h using a weighing machine (model AR2140, Essae Teraoka Ltd.) having an accuracy of 0.0001 g. The initial weight of HAP06Hr, HAP12Hr, HAP18Hr and HAP24Hr was 2.1 g, 2.08 g, 1.56 g and 1.82 g, respectively. The variation in the percentage of water absorption with time was plotted in **Fig. 4.14.** As observed, the W_a(%) decreases with

the increase in stirring timing from 6 to 24 h. The trend shows direct relation with the trend of porosity, relative density, and surface microhardness [163–165]. Also, the increase in the contact angle fundamentally replicates the decreasing trend of W_a (%). According to Baghbadorani et al. [166], to assess the biocompatibility of substances, water absorption testing simulates the conditions they would encounter within the oral cavity. Overabundance of water absorption could potentially lead to complications such as swelling, degradation, or modifications in mechanical characteristics, which could ultimately undermine the efficacy of the implant and its interplay with the surrounding tissues. Therefore, the test is essential to underline the effect of synthetic material in oral and orthopedic applications.

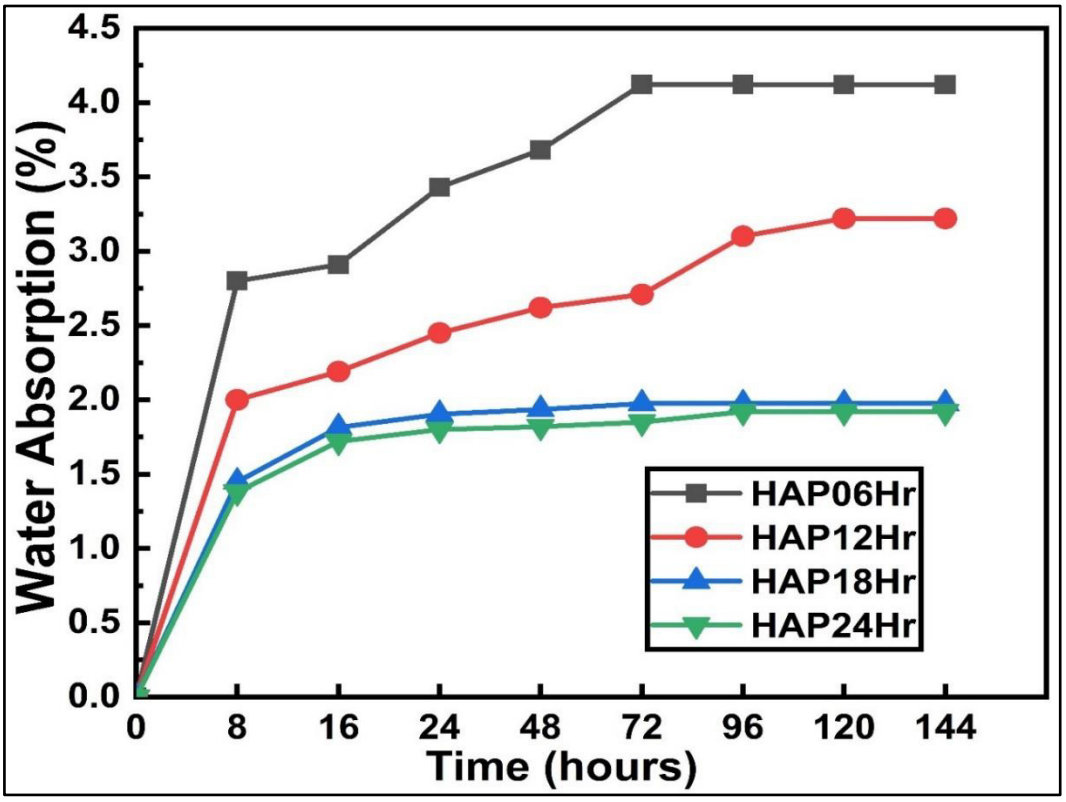

Fig. 4.14. Water absorption percentage of eggshell-derived HAp for 6 days.

4.2.5 Mechanical Characterization

4.2.5.1 Compressive strength

The compressive strength (CS) of the cylindrical HAp samples (size 1:2) prepared using cold pressing followed by sintering was examined using 25 kN servo controlled Universal Testing Machine (ASI Sales Pvt. Ltd) with aspect ratio 2, crosshead speed 1mm/min and under displacement control mode as per ISO 17162:2014 (for advance ceramics) standard. Three samples per compositions were used to determine the CS. The **Fig. 4.15 (a)** demonstrates the incremental movement of stress/strain curve till failure. As demonstrated in **Fig. 4.15 (b)**, the maximum compressive strength for HAP06Hr, HAP12Hr, HAP18Hr and HAP24Hr is 124 ± 1.0 MPa, 129 ± 1.80 MPa, 138 ± 1.20 MPa and 142 ± 0.6 MPa, respectively. Rao and Boehm [167] performed compressive test on the precipitated HAp samples sintered at 900-1200 ^{0}C for 0.5- 4 h. It was interesting to observe that, almost 99% similar result was obtained for HAP18Hr. However, the governing parameters, sample fabrication techniques and obtained morphologies plays a major role in the determination of MCS as illustrated by Metsger et al. [168] and Aminzare et al. [169]. Also, the young modulus depicts the increasing trend with increase in stirring timings.

Table 4.5. Maximum compressive strength and young modulus of eggshell-derived HAp at different stirring timings.

Sample	Maximum Compressive Strength (MPa)	Standard Deviation	Young Modulus (GPa)
HAP06Hr	124	1	5.23
HAP12Hr	129	1.8	5.38
HAP18Hr	138	1.2	5.54
HAP24Hr	142	0.6	5.61

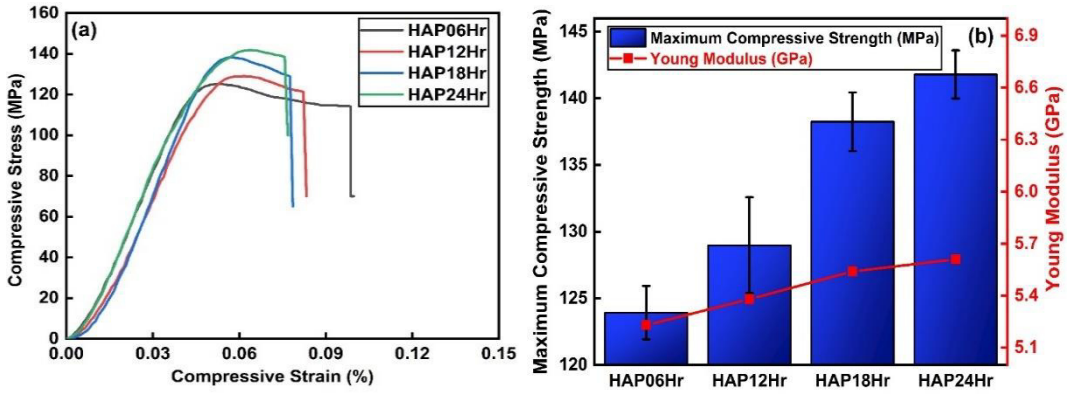

Fig. 4.15. (a) Compressive stress v/s strain diagram, and (b) Maximum compressive strength and young modulus of eggshell-derived HAp at different stirring timings.

The 7.26 % increase in young modulus was observed between HAP06Hr (5.23 GPa) and HAP24Hr (5.61 GPa) (**Table 4.5**). The densification, particle size reduction and the decrement in porosity [170] remarks the evidence for the increasing strength and resilience of the eggshell-derived HAp.

4.2.5.2 Vickers microhardness

Hardness characterization of the synthesized biomaterial is essential as it governs the durability, strength, wear resistance, biocompatibility and compatibility with manufacturing process. In the current research, the Vickers microhardness of the HAp samples was examined and analysed using Vickers Hardness Testing Machine (Mitutoyo, HM-200) with 5 inline indents per sample following ISO 6507-2 standard. The part programming panel with automatic measurement tool was used with pitch length 0.2 mm, normal load 100 g and dwell time 10 s. The values obtained were the average ± SD as shown in **Fig. 4.16**. As observed, the microhardness of HAP06Hr, HAP12Hr, HAP18Hr and HAP24Hr is 22.4 ± 0.4, 23.8 ± 0.6, 25.6 ± 0.5 and 26.10 ± 0.8 HVN, respectively. The increase in surface hardness with increase in stirring timing was observed and the probable reason for the increase could be the reduction in particle size [126], increased homogeneity of precipitation and densification of the structure [124]. These factors are amalgamated to increase the overall mechanical behavior of

the HAp samples. Wu et al. [171] determined the Vickers microhardness of radius bone obtained from human cadavers of three different donors and found the magnitude to lie between 25- 45 HVN. Therefore, the synthesized HAp can be used to replace the natural bone with the synthetic implant made of HAp. Also, the synthesized HAp has improved porosity as compared to natural bone and human tooth [32].

Table 4.6. Vickers microhardness of HAp samples.

Sample	Trial 1	Trial 2	Trial 3	Trial 4	Trial 5	Average	Standard Deviation	HVN Value
HAP06Hr	23	21.78	22.85	22.44	21.87	22.39	0.453	22.4 ± 0.4
HAP12Hr	23.8	24	24.87	23.56	22.7	23.79	0.639	23.8 ± 0.6
HAP18Hr	25.75	26.77	24.98	25.22	25.45	25.63	0.568	25.6 ± 0.5
HAP24Hr	26.11	25.65	24.87	26.1	27.78	26.10	0.870	26.1 ± 0.8

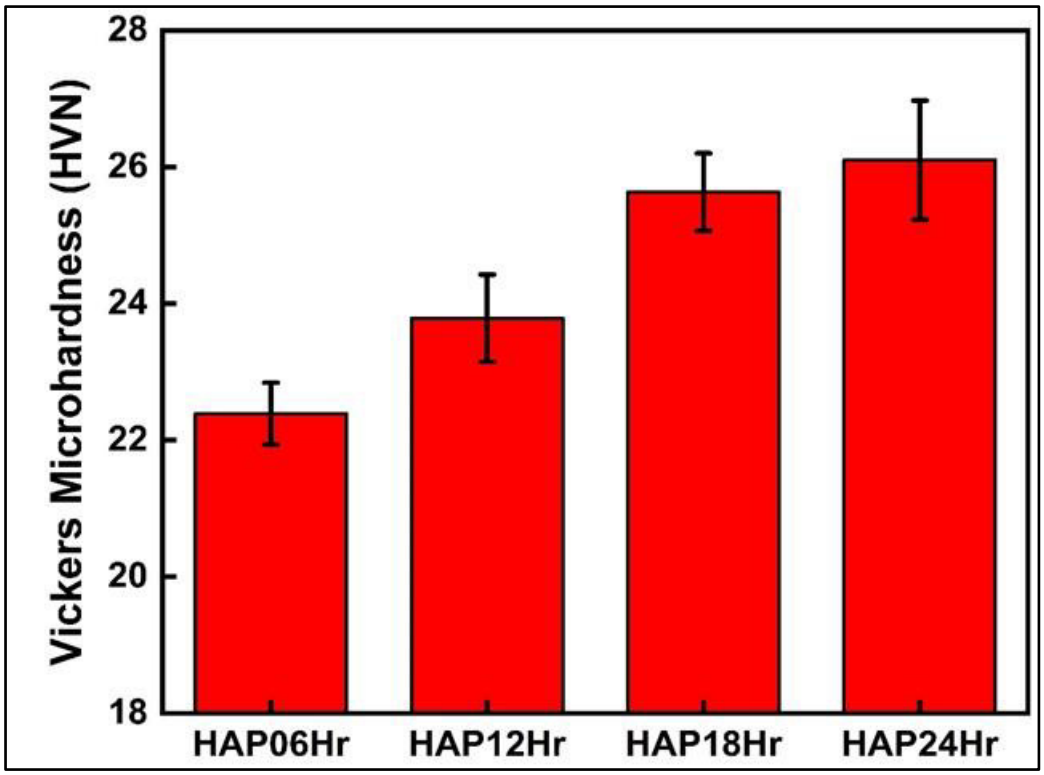

Fig. 4.16. Vickers microhardness of eggshell-derived HAp at different stirring timings.

4.2.6 Thermal Analysis

In order to characterize the thermal stability and decomposition behaviour of eggshell-derived HAp powdered samples, the thermogravimetric analysis was performed using TGA-50, by M/s Shimadzu (Asia Pacific Pvt. Ltd.). in temperature range of 32 ^{0}C to 1000 ^{0}C, ramping rate 10 ^{0}C/min, and under nitrogen-based inert atmosphere. The sample's weight at the beginning of experiment was HAP06Hr – 8.50 mg, HAP12Hr – 8.54 mg, HAP18Hr – 8.93 mg and HAP24Hr – 8.75 mg. The obtained results were plotted as weight remaining (%) v/s temperature as shown in **Fig. 4.17**. It was observed that stirring timing does not have much significant effect on decomposition rate or quantity and maximum 8% decomposition of HAp occurred when heated to 1000 ^{0}C. Comparatively, HAP18Hr has 0.32% less decomposition than HAP06Hr when quantified at 1000 ^{0}C. The initial degradation of approximately 1 wt% of synthesized HAp as the temperature increases from room tempersature to 300°C can be attributed to the removal of water molecules (i.e. dehydration) or other volatile substances that were physically and chemically absorbed within the structure. This phenomenon is widespread in many compounds, particularly those that have hydrated structures [24]. The sudden and substantial drop of ≈6.5 wt% of HAp between 375 ^{0}C – 500 ^{0}C reflects either a phase transition or a structural reorganization within the substance. The dihydroxylation process i.e. elimination of hydroxyl groups (-OH) from HAp lattice could be one of the potential reasons for the decomposition . However, higher thermal stability was observed, after 500 ^{0}C, till 1000 ^{0}C.

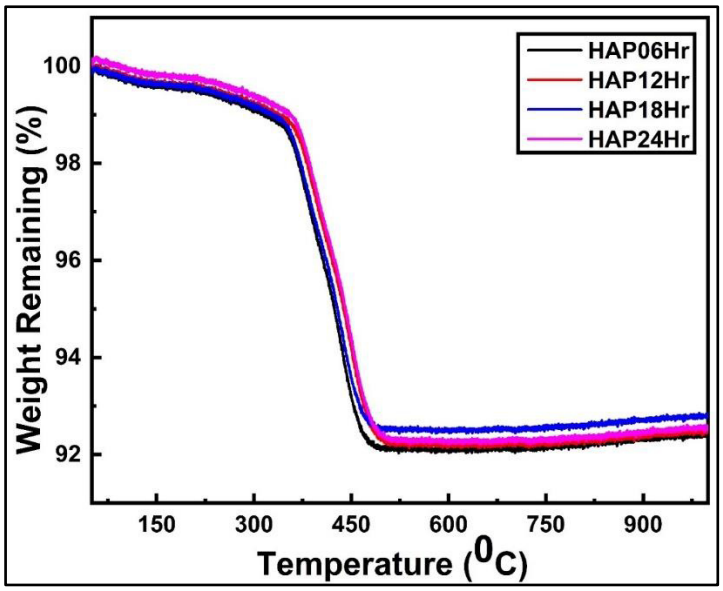

Fig. 4.17. Thermogravimetric Analysis of eggshell-derived HAp at different stirring timings.

In conclusion, the thermogravimetric analysis of eggshell-derived hydroxyapatite (HAp) demonstrates significant thermal stability and minimal decomposition, making it suitable for applications in orthopedic and dental implants. The decomposition behavior shows that the initial weight loss, up to 300°C, is likely due to dehydration and the removal of volatile substances. The primary decomposition occurs between 375°C and 500°C, indicating possible phase transitions or dihydroxylation processes. Beyond 500°C, the material exhibits remarkable thermal stability with only about 8% total weight loss at 1000°C, confirming the suitability of eggshell-derived HAp for high-temperature biomedical applications, where long-term durability and structural integrity are critical.